Journal of Alloys and Compounds 1002 (2024) 175223

Contents lists available at ScienceDirect

Journal of Alloys and Compounds

journal homepage: www.elsevier.com/locate/jalcom

Nanostructured FeCo films of exceptionally high saturation magnetisation

Raúl López-Martín [a,*], Chris Binns [a], Benito Santos Burgos [a], Peter S. Normile [a], José A. De Toro [a], Andrew Pratt [b], Toby Bird [b], Maha Alotaibi [b,c], Jack Pearce [b], David Hesp [b], Connor Fields [d], Shengfu Yang [e], Hanqing Liu [e], Larissa S.I. Veiga [f], Sarnjeet S. Dhesi [f]

[a] Instituto Regional de Investigación Científica Aplicada (IRICA) & Departamento de Física Aplicada, Universidad de Castilla-La Mancha Ciudad Real, Ciudad Real 13005, Spain
[b] School of Physics, Engineering and Technology, University of York, YO10 5DD, UK
[c] Department of Physics, College of Khurma University College, Taif University, P.O. Box 11099, Taif 21944, Saudi Arabia
[d] School of Physics and Astronomy, University of Nottingham, NG7 2RD, UK
[e] School of Chemistry University of Leicester, LE1 7RH, UK
[f] Diamond Light Source, Rutherford Appleton Laboratory, Didcot OX11 0DE, UK

ARTICLE INFO

Keywords:
Nanomaterials
FeCo Nanoparticles
Magnetic Films

ABSTRACT

Nanostructured FeCo films comprising small (2.1 nm mean diameter) Co nanoparticles deposited into an Fe matrix are investigated by magnetometry, transmission electron microscopy and X-ray Magnetic Circular Dichroism (XMCD). Similar films were previously reported to possess a saturation magnetisation of up to 3 μ_B/atom, thus exceeding the Slater-Pauling limit by a significant margin. The present work confirms the previous findings by magnetometry and demonstrates that the Co nanoparticles maintain their particulate identity within the film while adopting the crystallographic structure of the Fe matrix. The films show no evidence for voids or porosity (they exhibit the bulk density). An important factor in the high magnetisation in the films is an enhanced magnetic moment on the Co atoms, which XMCD indicates to be at least 2.21 μ_B, i.e., 30 % larger than the bulk value for metallic cobalt.

1. Introduction

In a world increasingly electrified, there is an urgent requirement to develop soft magnetic materials with a higher saturation magnetic flux density, defined as $B_s = \mu_0 M_s$, where M_s is the saturation magnetisation, than those currently available. For over a century, the highest value of B_s available in a soft bulk material has been 2.45 T -found in FeCo alloys- and is referred to as the Slater-Pauling limit (SPL). This extraordinarily high magnetisation was first discovered in 1912 [1]; subsequent work on processing has improved the mechanical properties and magnetic softness of the material but the maximum value of B_s has remained the same [2]. The SPL has represented a limit to performance in a number of industrial applications, so finding a material with a B_s value that exceeds such limit is an important challenge for applications.

One of these applications is magnetic recording, where a material with higher B_s (at the tip of the writing pole) would enable the use of a more anisotropic granular medium. This, in turn, would help to circumvent the superparamagnetic limit and overcome the so-called 'magnetic recording trilemma' [3,4]. Thus, such a material could increase the current magnetic recording density. Another example where materials with high magnetisation are needed is the development of all-electric transport required for a low carbon economy. Reluctance electric motors have at their heart a soft magnetic material that is magnetised by an applied field and the torque developed by the motor is proportional to M_s [5]

According to a recent, comprehensive review of all progress in the synthesis of high-moment materials [6], FeCo remains the bulk soft magnetic material with the highest room temperature value of M_s more than a century after its discovery. The behaviour of these alloys can be understood in terms of the changing position of the Fermi level within a spin-split rigid band structure, as the average electron spin polarization at the Fermi level is altered by the proportion of Co [7]. Such behaviour of the bulk alloy can be accurately modelled by first principles calculations [8].

Although higher values of M_s are observed in bulk rare-earth materials, these are unsuitable for soft magnetic material applications due to

* Corresponding author.
E-mail address: raul.lopez@uclm.es (R. López-Martín).

https://doi.org/10.1016/j.jallcom.2024.175223
Received 2 April 2024; Received in revised form 6 June 2024; Accepted 16 June 2024
Available online 17 June 2024

their low Curie temperature and high coercivity. All other materials described in the review of high moment materials [6] are *ultra*-thin molecular beam epitaxy (MBE) films, whose performance relies on fine crystallographic matching and would not have a clear upscale path. This includes $F_{16}N_2$, which can have a saturation flux density of up to 2.9 T in MBE-grown ultra-thin films, but the B_s value reduces to 2.3 T when attempting to go to the bulk [9]. In addition, $F_{16}N_2$ is not magnetically soft. As a further illustration of the difficulty of moving beyond the Slater-Pauling limit, a recent study using a machine learning approach to comprehensively search FeCo alloy compositions with added impurities discovered, after running for months, that adding small amounts of Ir and Pt could produce only a small (3.5 %) enhancement of the maximum B_s value [10].

The most promising material reported so far with a magnetisation beyond the SPL at room temperature is *nanostructured* FeCo produced by depositing size-selected gas-phase Co nanoparticles in conjunction with an atomic Fe vapour [11]. This synthesis method produces nanoparticles embedded in an atomic matrix as illustrated in Fig. 1**b**. Due to the nanostructure, which randomizes the magnetic anisotropy axes of the embedded nanoparticles, these films are also magnetically soft and present robust magnetic behaviour [12,13], which means that the synthesis is easily scalable. In general terms, this high B_s can be understood as the result of size effects in small clusters coated with a second magnetic transition metal.

As has been known for decades, free nanoparticles exhibit significantly increased magnetic moments per atom compared to the bulk value for all the transition metals [14–17], reaching 5.5 μ_B/atom in sufficiently small Fe clusters, which is close to the atomic limit [16]. X-ray Magnetic Circular Dichroism (XMCD) measurements of size-selected Fe nanoparticles deposited on graphite showed a significant increase in the magnetic moment per atom over the bulk value for sizes below about 700 atoms, with nearly half of the enhancement coming from the orbital magnetic moment [18]. Interestingly, coating the exposed Fe nanoparticles with Co does not diminish the enhanced orbital moment and increases the spin magnetic moment even further [18]. This suggested that co-deposition of small size-selected nanoparticles of either Co or Fe with an atomic vapour of the other material to form a nanostructured film could lead to a high-moment material in which the enhanced moments were preserved [11].

It was found, however, that for films with nanoparticle volume fractions (or nanoparticle concentration) above the percolation threshold, the average magnetic moment per atom in the film drops to a weighted average of the Fe and Co moments, while at lower volume fractions the magnetisation in the film is above the Slater Pauling curve for the conventional alloy. The highest moments were observed at the Fe-rich end (Co nanoparticles in a metallic Fe matrix).

There remains, however, a lack of detailed knowledge of the origin of the high moments in these systems. In the present work we revisit this system, focussing on the Fe-rich end of the composition curve by depositing size-selected Co nanoparticles and Fe atomic vapour at different concentrations of nanoparticles. Our study *confirms* the high magnetisation of these systems. By combining electron microscopy, magnetometry and X-ray Magnetic Circular Dichroism (XMCD) measurements, we have obtained a detailed picture of their structure and magnetic properties.

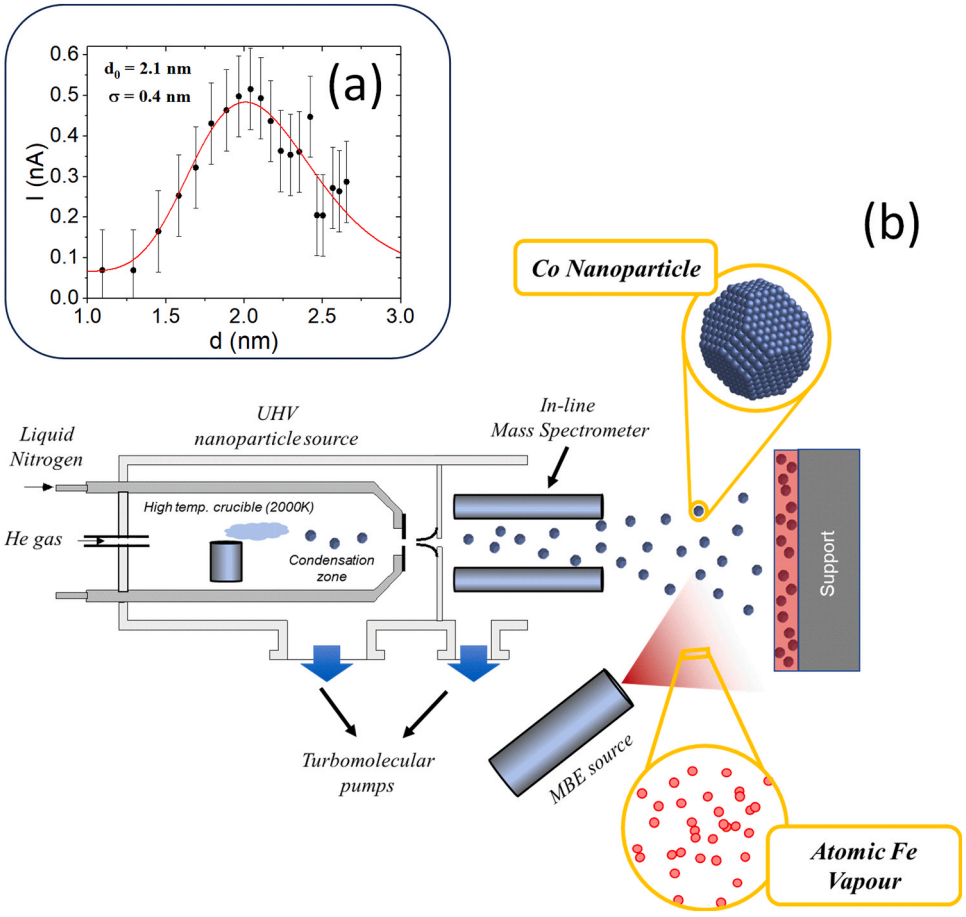

Fig. 1. (a) Typical mass spectrum of Co clusters. **(b)** Synthesis of nanostructured FeCo films by co-depositing Co nanoparticles in conjunction with an atomic Fe vapour.

2. Materials and methods

2.1. Synthesis of nanostructured FeCo films

All the magnetic films were synthesised using an ultra-high vacuum (UHV) thermal nanoparticle source at the School of Physics, Engineering and Technology, University of York. The source is described elsewhere [19]. The crucible was loaded with Co and the nanoparticles were deposited onto substrates in a UHV deposition chamber (base pressure of *ca.* $3x10^{-10}$ mbar) in conjunction with an Fe vapour produced by a Molecular Beam Epitaxy (MBE) source as illustrated in Fig. 1**b.**

The nanoparticle source is equipped with an in-line high mass quadrupole mass spectrometer to determine the size distribution of the deposited particles. Fig. 1**a** shows a mass spectrum of the Co nanoparticles fitted to a log-normal distribution with a peak value of 2.1 nm and $\sigma = 0.4$ nm. For magnetometry characterization, FeCo films with a thickness of around 50 nm were deposited onto polyetheretherketone (PEEK) substrates with 50 nm Ag buffer and capping layers either side of the magnetic layer. The capping layer was thick enough to prevent oxidation as no trace of oxides could be inferred or detected in magnetometry measurements or energy dispersive X-ray (EDX) analysis (see Section 2.3). For the XMCD experiments, the 50 nm FeCo films were deposited onto Cu substrates with a 1 nm Cu capping layer, sufficiently thin to allow X-ray Absorption Spectroscopy (XAS) using total electron yield (TEY), as described in Section 2.5, but not thick enough to prevent slight surface oxidation of the films. The nominal film thicknesses of all elements were determined in situ using a quartz crystal monitor (QCM) installed in the deposition chamber. The true thicknesses were determined by calibrating the QCM as described below. The thickness and compositions of some of the films produced for magnetometry on PEEK substrates were determined by electron microscopy on lamella produced by a focused ion beam (FIB) instrument, as described in Section 2.3.

2.2. Determining the amount of Fe and Co in the films

To convert the measured magnetic signal at saturation to total magnetic moment per atom in the film, the precise amount of Fe and Co in the samples needs to be known. However, the nominal film thicknesses measured in situ by the QCM were not sufficiently accurate to extract reliable values. Two different experiments were therefore carried out to calculate a calibration factor for the QCM, one for the Fe atomic vapor and another for the Co clusters. To calculate the calibration factor that helps extract reliable values of the number of Fe atoms, a pure Fe sample (sample 1 in Table 1) was measured by SQUID magnetometry. From the saturation magnetic moment, the mass and thus the number of atoms can be calculated assuming both the bulk magnetisation and the bulk density. The ratio between the number of atoms obtained by magnetometry and the number of atoms from the QCM yields the calibration factor that, in this study, is 0.80 ± 0.04. The error in this calibration factor arises from the fact that the Fe deposition was only measured before and after the film was produced and the average was taken. The difference between those values is typically 5 %. The value of the calibration factor was confirmed by local measurements of the thickness of an Fe film cross section by SEM in an Fe/Si sample (sample 8 in Table 1). The thickness measured by using SEM, averaged from 8 different positions on the film was 82 ± 8 nm, while the nominal thickness was 93.8 nm, giving rise to a calibration factor of 0.87 ± 0.10 for the QCM. Note that as the Fe film is continuous, a difference in mass will translate to a difference of thickness. As the calibration factors agree within the error bars, the one obtained from magnetometry is taken as this measurement provides a more reliable average over the whole sample.

To obtain the corresponding Co calibration factor, XAS measurements in sample 7 (see Section 2.5) were used. They showed that the ratio of Co and Fe calibration factors was 0.57, which, using the above factor for Fe, yields a factor of 0.46 for Co alone. Note that such a low QCM calibration factor is normal for highly porous nanoparticle assemblies. The error in this factor was also taken as the difference between the initial and final deposition rate, this being a 20 % difference. Using these two calibration factors, the samples produced in this work and their calibrated Co atomic content are summarized in Table 1.

2.3. Electron microscopy of the nanostructured films

To obtain electron microscopy images of the films, cross sections were prepared by focused ion beam (FIB) lift out. The films were placed on FIB stubs using carbon tabs and a very thin layer of Cu (~4 nm) was sputtered on top to help with charging during the thinning procedure, for which, an FEI Nova 200 FIBSEM was used. Firstly, a Pt mask was deposited (via gas injection) on top of the sample to around 2 μm in thickness to protect the lamella. A liquid metal source provided the Ga ions used to trench the sample around the Pt mask. A needle using a Kleindiek 3-axis micro-manipulator was brought into contact with the lamella where it was attached using a small quantity of Pt. The lamella was then fully cut out from the sample and lifted out using the needle where it was attached onto a Cu grid with more Pt and the needle cut free using Ga ions. The lamella was then progressively thinned with the Ga ions to provide electron transparency for imaging in the electron microscopes.

Once the lamella was lifted out and placed on the Cu supporting grid, it could be imaged on a scanning electron microscope (SEM). A JEOL JSM7800F SEM was used for the measurements which is equipped with dual Oxford Instrument EDX detectors. The lamella was placed at a normal angle to the beam and detectors such that the whole cross-section could be viewed in the imaging plane allowing for thickness measurements of the grown FeCo films. EDX measurements of the individual layers was also possible in this arrangement. The imaging was typically performed with electron beam energies of 5–30 keV.

Transmission electron microscopy (TEM) imaging was performed on a JEOL 2100+ utilising a single tilt sample holder. EDX maps were taken with an Oxford Instruments EDS detector placed in-plane with the sample with imaging during acquisition performed in STEM mode. The electron beam is formed by a LaB_6 filament with beam energies of 200 keV. This instrument allowed the effective imaging of the FIB cross-section with bright field images, diffraction, and EDX maps to be taken at higher magnification and resolution than the SEM.

In the case of the calibration sample deposited onto Si, the film was carefully cut with a diamond blade and the cross section was imaged by

Table 1
Samples prepared by cluster deposition on different substrates with a Ag buffer layer of 50 nm (in each case).

Sample	Thickness (nm)	Composition (at% Co)	Substrate	Capping layer	Measurement
1	40.4 ± 2.0	0	PEEK	Ag (50 nm)	SQUID
2	38.0 ±1.9	1.3±0.3	PEEK	Ag (50 nm)	SQUID
3	40.8 ± 2.0	3.5 ± 0.7	PEEK	Ag (50 nm)	SQUID/TEM
4	34.6 ± 1.7	5.6 ± 1.1	PEEK	Ag (50 nm)	SQUID
5	34.7 ± 1.7	8.0 ± 1.6	PEEK	Ag (50 nm)	SQUID/VSM
6	34.5 ± 1.7	11.4 ± 2.3	PEEK	Ag (50 nm)	SQUID/VSM
7	35.4 ± 1.8	10.9 ± 2.2	Cu	Cu (1 nm)	XMCD
8	75.0 ± 3.8	0	Si	Ag (50 nm)	SEM

a ZEISS GeminiSEM 500 FESEM at electron energies of 2 keV.

2.4. VSM and SQUID measurement of the magnetic behaviour of the films

Most magnetic measurements were performed in a Quantum Design EverCool MPMS XL SQUID magnetometer at the Universidad de Castilla-La Mancha, Spain. The films were rolled into the sample holder to measure the in-plane response of the samples. In the case of samples 4 and 6, the films were rolled in a PEEK capsule which was mounted in the sample holder. Hysteresis loops were recorded at 300 K and 5 K using magnetic fields up to 50 kOe. The 5 K loop was recorded after cooling the sample in a saturating field of 50 kOe to look for the presence of exchange bias as a fingerprint of Co oxidation. Diamagnetic contributions of the substrate and the sample holder, in addition to that of the PEEK capsule (if used), were subtracted. In some cases, to measure the coercivity of the films, a second loop was recorded, where the saturating field used was much lower (2 kOe) due to the soft response of the sample. In all the cases the loops fulfilled the major loop criterion [20].

Some magnetic measurements were also obtained from the films rolled into PEEK capsules using an ADE Model 10 vibrating sample magnetometer (VSM) at the University of York, UK with the field applied out of plane (see upper inset in Fig. 4)

2.5. XMCD measurements of the orbital and spin magnetic moments

The XMCD measurements were taken on beamline I06 at the Diamond Light Source, UK. The beamline provides circularly polarised X-rays in the photon energy range 106 – 1300 eV from an undulator source. The XMCD end station is equipped with a 6 T superconducting magnet that enables measurements on samples at temperatures down to 1.5 K. In the measurements reported here, the temperature of the sample was at the ambient value of the sample space within the superconducting magnet, which settled at around 200 K. The films were fully saturated at 6 T at this temperature. The absorption spectra were recorded using TEY mode with a photoelectron detector. No self-absorption corrections were made as the escape depth of photoelectrons is about 2 nm. To simplify the analysis using sum rules, all measurements were made with a photon incidence angle, relative to the sample normal, of 55°, which, within certain assumptions, eliminates the dipole term from the spin sum rule [21,22].

3. Results

3.1. Structure of the films determined by electron microscopy

Electron microscopy images were obtained from a lamella produced by the FIB lift-off technique described in Section 2.3. Fig. 2**a** shows an SEM image of the cross section of the film with 3.5 at% Co (sample 3 in Table 1), revealing the trilayer Ag/FeCo/Ag sandwich with the Pt coating deposited for the FIB lift-out and the PEEK substrate. In this image the Fe EDX signal has been highlighted in pink to show the region containing Fe. Fig. 2**b** shows a zoom-in on the Ag/FeCo/Ag trilayer. Higher resolution EDX maps for the four elements of interest, that is, Ag, Fe, Co, and O in a region of the trilayer are shown in Fig. 2**c**. It is clear that the Fe and Co are contained in the central part of the trilayer with no evidence for interdiffusion and that the oxygen signal is negligible. The small trace of oxygen detected in the central part of the lamella (faint green band in the lower right panel of Fig. 2**c**) may originate during FIB lift-out.

A TEM image of a lamella from sample 3 with the Ag layer thinned down is shown in Fig. 3**a**. The lower resolution image shows the complete film and the expansion clearly shows a grain structure with the yellow outline indicating the size of a single Co nanoparticle, which is similar to the grain size evident in the image. An important observation is that there is no evidence for voids in the film and that the atomic matrix completely fills the gaps between the nanoparticles. Fig. 3**b** shows a diffraction pattern, which contains only bcc reflections with the Fe lattice constant, i.e., 2.84 Å. This is in agreement with previously published EXAFS data on films of embedded Co nanoparticles in Fe matrices that shows that the Co nanoparticles adopt the bcc Fe lattice up to a volume fraction of 40 % (42 at% Co) [23].

3.2. VSM and SQUID magnetometry

The samples produced on PEEK substrates were rolled into cylinders as sketched in the upper inset in Fig. 4. The hysteresis loops from samples 1 – 6 in Table 1 were measured by a SQUID magnetometer with the field applied along the cylinder, that is, in-plane to the films, in the range −50 to +50 kOe and at temperatures of 5 K and 300 K. In addition, hysteresis loops were obtained using a VSM from samples 4 and 6 with the applied field across the cylinder, *i.e.*, at all incidence angles relative to the film plane in the range −15 to +15 kOe at 300 K. All the loops from samples containing Co look similar and representative curves from sample 6 are shown in Fig. 4.

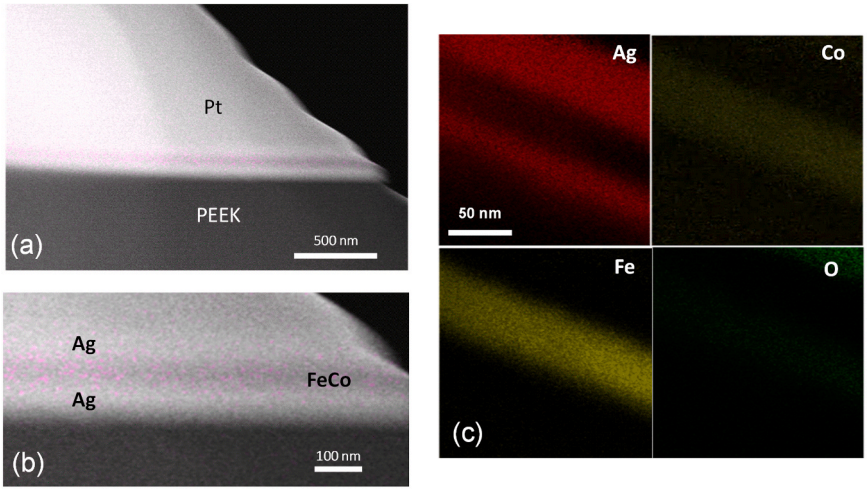

Fig. 2. **(a)** Film cross section (sample 3) after FIB lift out revealing the trilayer Ag/FeCo/Ag on PEEK and the Pt layer used during the production of the lamella. The Fe EDX signal has been superimposed. **(b)** Zoom-in on the trilayer region where the FeCo film and the Ag capping and buffer layers are seen. **(c)** Higher resolution EDX element maps of the four elements of interest, that is, Ag, Fe, Co, and O in a region of the trilayer.

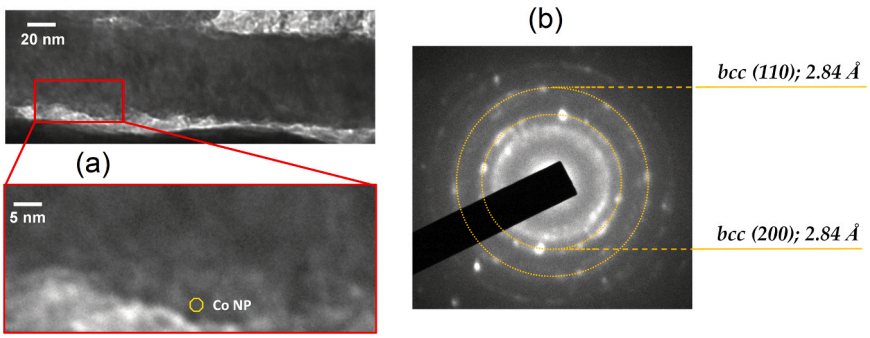

Fig. 3. **(a)** TEM image of the film cross section. The yellow outline in the lower image shows the size of a single Co nanoparticle. **(b)** Electron diffraction from the lamella showing a bcc structure with the Fe lattice constant.

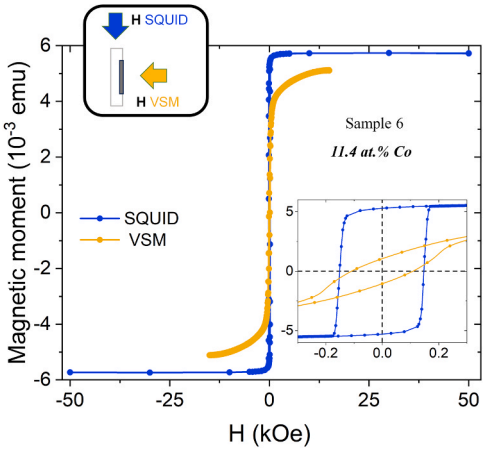

Fig. 4. Magnetic moment vs. applied magnetic field from sample 6 measured with the two different magnetometers at 300 K. The SQUID field was applied in plane and the VSM field across the cylinder as shown in the upper inset. The lower inset shows the low field region.

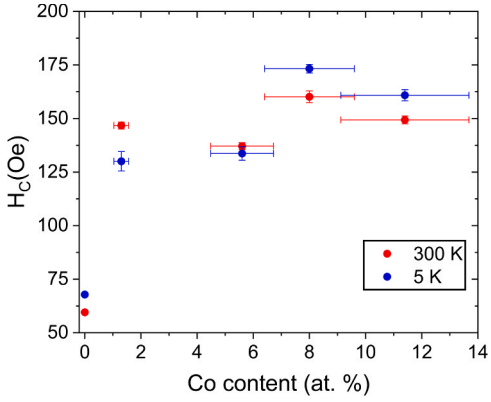

Fig. 5. Coercivity vs. Co content for all the samples at 5 K and 300 K.

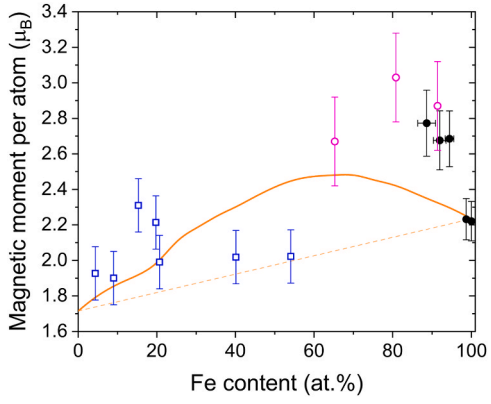

Fig. 6. Magnetic moment per atom for films of Co nanoparticles in Fe matrices. Filled circles: new data reported here, open circles: previous data [11]. Open squares show previous data for Fe nanoparticles embedded in Co [11]. Also shown is the Slater-Pauling curve for conventional alloys (orange full line), while the dashed line indicates the weighted average of the Fe and Co moments.

The SQUID data shows saturation at relatively low fields while the magnetic moment out of plane of the sample is not saturated even at the maximum available field from the VSM of 15 kOe. These differences indicate that the films have in-plane magnetic anisotropy rather than perpendicular magnetic anisotropy as expected for FeCo thin films [24, 25]. As the SQUID field is applied parallel to the film, lower fields are needed to align the magnetic moments and thus to saturate the magnetic response. The lower inset in Fig. 4 shows the low-field region of the loops. In both configurations a similar coercivity in the region of 100 – 150 Oe is observed. No horizontal shift, *i.e.* exchange bias effect, was found in any of the samples, indicating that no significant oxidation of the Co nanoparticles took place.

The coercivity for in-plane magnetisation as a function of Co content at 5 K and 300 K is shown in Fig. 5. It is observed that the coercivity of the pure Fe film is close to zero and that the addition of Co increases the coercivity to around 150 Oe. Within the error, the coercivity of the nanostructured films is almost independent of Co content and temperature. Although the coercivity is quite low, it is not in the range of what would normally be considered a soft material for applications (see Fig. 1 in [26], where the typical maximum coercivity is 1 kA/m, *i.e.*, 13 Oe).

The most important information derived from the magnetometry data is the magnetic moment per atom, which is obtained from the saturation magnetic moment together with the amount of Fe and Co in the samples, using the calibration procedure described in Section 2.2. The saturation magnetic moment was taken as the value at the maximum applied magnetic field in the SQUID magnetometer (50 kOe) with the sample at 5 K. The results are shown by the filled circles in Fig. 6 and compared to previous data, depicted by open squares and circles from films synthesised using the same cluster deposition technique [11]. The orange full line is the Slater-Pauling curve for the magnetisation in conventional alloys as a function of the Co content, obtained from the experimental points in [27]. The open blue squares in Fig. 6 are the values obtained from films of Fe nanoparticles deposited in conjunction with Co matrices while the open pink circles show values from films of Co nanoparticles deposited in conjunction with Fe matrices. At the Co rich end, the magnetic moment per atom is higher than the Slater-Pauling curve but at Fe nanoparticle content beyond the percolation threshold of 25 % (corresponding to 75 at% Co), the

moment drops to the weighted average of the Fe and Co moments, shown by the dashed line. At the Fe-rich end, explored by depositing Co nanoparticles in Fe matrices, for nanoparticle content below the percolation threshold, the magnetic moment per atom is higher than the Slater-Pauling curve and reaches values higher than the SPL. Our new data (filled circles), with lower error bars agrees, within error, with the previous data and confirms that this material has a magnetisation beyond the SPL. The uncertainty in concentration derives mainly from the uncertainty in the QCM calibration factor for Co (see Section 2.2) while the vertical error bars derive from the uncertainty in the determination of both Co and Fe number of atoms.

3.3. X-ray magnetic circular dichroism

XAS and XMCD over the Fe and Co *L* edges are depicted in Fig. 7. They were measured from sample 7 (10.9 at% Co content), at a temperature of 200 K and an applied field of 6 T. XAS at the Fe edge (inset of Fig. 7**c**) shows a two-peak structure with the main peak at around 710 eV as is observed in other studies of partially oxidised granular Fe films [28]. Fe oxides all show a similar multiplet structure with a main peak at around 709–710 eV and a shoulder around 707 eV [28]. Yet, the strong dichroism (around 30 %) at 707 eV compared with the weaker dichroism of the main peak indicates that this signal belongs to the metal Fe species, also expected at 707 eV in granular systems [28]. Given the surface sensitivity of XAS measured by TEY, probing just the first 1–2 nm of the film, any surface oxide will be emphasized in the spectra. In our work the surface oxidation is produced *ex-situ* as the 1 nm Cu layer is not able to prevent oxidation.

Despite the strong dichroism of the pure Fe signal, extracting quantitative values of the atomic magnetic moments of the Fe atoms is not feasible as the Fe oxides still accounts for the majority of the XAS. Thus, the dichroic shoulder ascribed to metal Fe sits on a significant contribution from the weakly dichroic signal of the oxides, precluding a reliable quantification.

On the other hand, XAS and XMCD in the Co L edge were dominated by the clean metallic-like signal, with only a very slight trace of oxide. This is not unexpected since the standard potential of Co is −0.28 eV compared to −0.44 eV for Fe, thus in a mixed system the oxygen will tend to reside within the Fe portion. The small shoulders evident in the Co L_3 edge XAS spectra (Fig. 7) are due to oxide species of very low proportion (bearing in mind that in a fully oxidised sample, the shoulder just above the L_3 edge would be as intense as the main peak [29])

The steps in the processing of the raw data to obtain the integrals required for the sum rule analysis are shown in Fig. 7. First, the raw data were fitted with a linear background to ensure that the edge integral starts from zero (Fig. 7**a**). Then, an integral background was fitted under the L_2, L_3 absorption peaks (Fig. 7**b**) to obtain the clean dichroic absorption edge signal shown in Fig. 7**c**. This was then integrated to obtain the integrals (P, Q and R) required for the sum rule analysis, as shown in Fig. 7**d**. Both Q and R integrals are reasonably well converged by the end of the spectra and would be expected to provide a reliable value for the orbital and spin magnetic moments on the Co. It is notable that the L_3/L_2 branching ratio, defined as $I_{L3}/(I_{L3} + I_{L2})$, where I_{L3} and I_{L2} are the integrated intensities over the L_3 and L_2 peaks respectively, differs from the bulk value, as expected in nanoparticles. The bulk value is 0.70 while in Co nanoparticles it is found to vary between 0.70 and 0.77 as a function of particle size [30]. We obtain a value of 0.74 in our samples, indicating that the Co is indeed in the form of nanoparticles. The branching ratio also changes with the level of oxidation [31], but such effects are much less significant than the size effect.

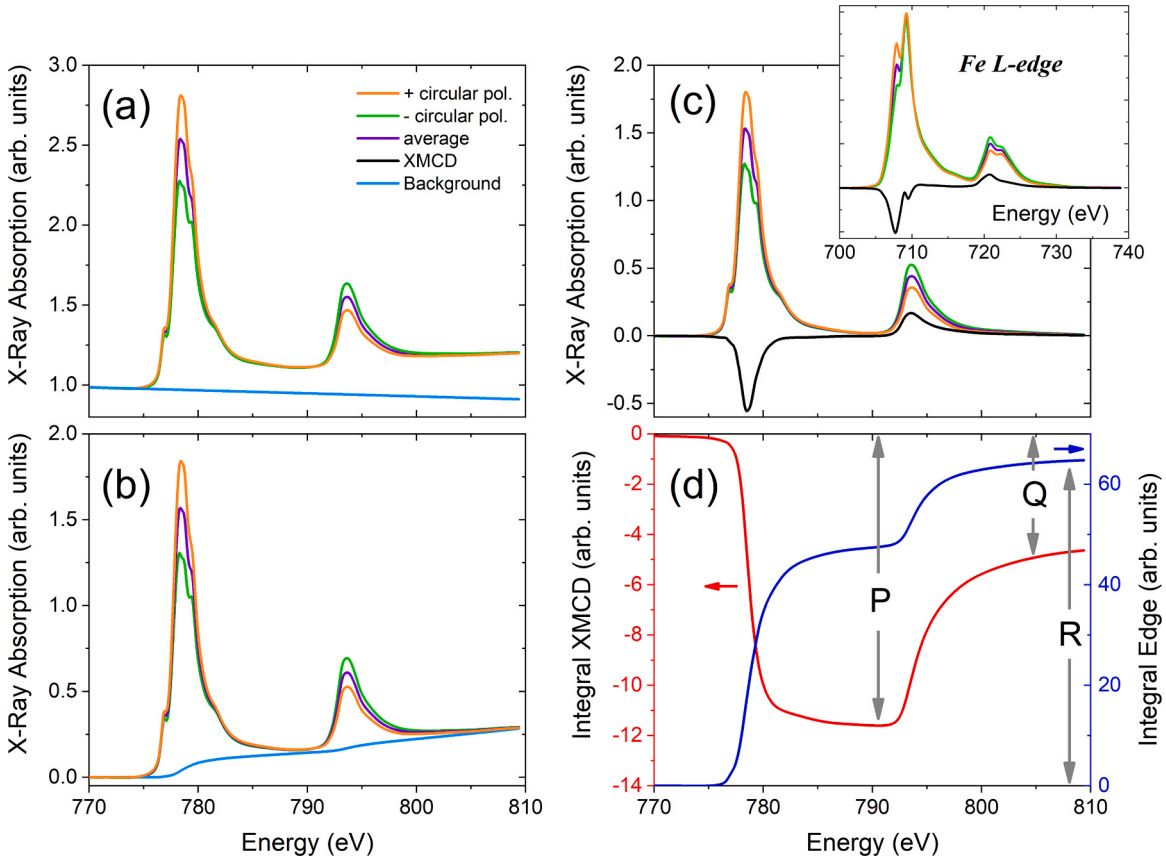

Fig. 7. **(a)** X-ray absorption at the Co L edge at both circular polarisations and the average along with the fitted linear background to the pre-edge region (sky blue line). **(b)** Fitted integral background under the L_3 and L_2 peaks. **(c)** background subtracted spectra and the X-ray dichroism. The inset shows the XAS and XMCD at the Fe edge **(d)** Integrals of the XMCD spectrum and the total edge absorption.

The sum rules apply only at magnetic saturation and to confirm that the sample was magnetically saturated at 200 K and 6 T, the dichroism was measured at the L_3 edge of both the Fe and Co edges at 200 K as a function of the applied field. The resulting magnetisation curves are shown in Fig. 8. Since the Fe is oxidised, it is not worth commenting on the differences between the Fe and Co magnetisation. The Co edge dichroic signal is significantly weaker than that of Fe, which accounts for the noisier Co magnetisation curve compared to Fe. However, it is clear that both magnetic (elemental) components are saturated at 6 T (60 kOe). Also superimposed for comparison is the magnetisation curve obtained using the SQUID magnetometer from sample 6, which has a similar composition to sample 7. This curve saturates at lower field values since the magnetisation was applied in the film plane during SQUID measurements, as opposed to 55° out of plane during the XMCD measurement. Note that as TEY was used to obtain the absorption spectra, only the first few nanometres were probed as opposed to the 'bulk' magnetisation, measured with the SQUID magnetometer.

The orbital and spin moments of the Co atoms in sample 7 can be obtained by applying the sum rules derived for L edge circular dichroism [32,33]. In addition to the orbital and spin moments, the sum rules contain a dipole term that is a measure of the anisotropy of the spin distribution and is present in XMCD measurements since the photon polarisation samples a directional cut through the atomic electron density. It manifests itself as a dependence of the spin moment on angle and although it is small in bulk samples, it cannot always be neglected in thin films and nanostructures. However, it was shown that in a thin film with rotational symmetry parallel to the substrate surface, the dipole contribution becomes vanishingly small when the X-ray beam is incident at 55° to the sample normal [21,22], which was, thus, the selected geometry in all our XMCD measurements.

Ignoring the dipole term, the effective sum rules for the L edge in a transition metal predict the orbital, m_L, and spin, m_S, moments in terms of the integrals shown in Fig. 7**d**:

$$m_L = \frac{4}{3}\frac{Q}{R}n_h$$

$$m_S = \left(\frac{6P - 4Q}{R}\right)n_h$$

The term n_h is the number of holes at the Fermi level, which in a transition metal is not an integer. In the bulk, the number is 2.5, while for very small clusters, it is in the range 2.3 – 2.5 [34]. The value was found to converge to the bulk one for clusters with more than 15 atoms, thus we use the bulk value in the analysis here. This gives, for Co, $m_L = 0.24\ \mu_B$, $m_S = 1.97\ \mu_B$ and for a more than half-filled 2p shell, the two are added to give a total atomic magnetic moment, m_T, of 2.21 μ_B, which constitutes a 30 % enhancement with respect to the 1.7 μ_B value for bulk Co. This measured value is as high as that found in vacuum for free Co clusters of about the same size as the nanoparticles in our sample [35], which, crucially, are embedded in a material. This can be considered as a lower limit since the slight oxidation will reduce the measured moment.

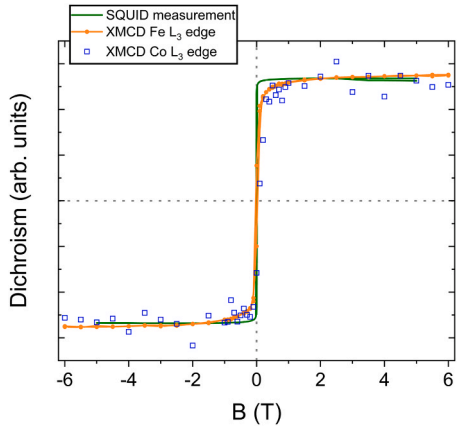

Fig. 8. Applied field dependence of the dichroic signals at the Co and Fe L_3 edges measured at 200 K. The green line is the hysteresis loop of the same sample measured in a SQUID magnetometer in an in-plane configuration (compared to 55° out of plane in the case of the XMCD measurements).

4. Discussion

The multi-technique study of this nanostructured FeCo material has enabled a better understanding of its magnetic performance. The structural studies have shown that the Co nanoparticles maintain their particulate identity within the film (Fig. 3**a**) but adopt the bcc atomic structure with the lattice constant of Fe (Fig. 3**b**). In addition, there is no evidence for voids in the films, i.e. the Fe matrix atoms pack tightly round the Co nanoparticles producing a film with the bulk density. At a Co content greater than a few percent, the Fe matrix will also form a nanostructure interfaced to the Co so the basic premise that the material consists of an interacting nanoparticle assembly is reasonable. Note that, for the maximum volume fraction attained in this work (ca. 11 % Co), the probability of having cluster-cluster contacts is small and the Co interfacial atoms can be estimated by assuming that the outer shell of Co atoms have a thickness equal to the lattice parameter (i.e. 2.84 Å). For the Fe interfacial atoms, a shell of atoms surrounding the Co cluster with a thickness equal to the lattice parameter can be assumed. From these estimations, 60 % of Co atoms are interfacial while 15 % of Fe atoms in the matrix are interfacial. Close to the percolation threshold (ca 20 % Co), the interfacial Fe atoms would increase to 30 % of the Fe atoms in this simple model.

Even though the magnetic moment of the Co atoms, as observed by XMCD is higher than the bulk value, the majority of enhancement in the magnetisation compared to bulk FeCo alloy must be coming from an increased magnetic moment on the Fe atoms. This hypothesis is supported by the study of Xie and Blackman [36], who found that Fe atoms in core-shell Fe@Co clusters with the composition Fe_nCo_{1021-n} had a magnetic moment of 2.5–2.6, μ_B depending on the core size, n. In addition, measurements of the spin and orbital moments of Fe atoms in Fe nanoparticles in the size range 200 – 400 atoms deposited on graphite and coated with Co revealed a total magnetic moment per atom of around 2.5 μ_B [18]. This is still not as high as the highest value indicated by magnetometry here (2.77 ± 0.18 μ_B/atom), but in the previous work only one side of the nanoparticles was coated in Co, the other being in contact with graphite.

The origin of this enhancement of the magnetisation may come from the Fe-Co interface where a strong hybridization from the d bands of both the Fe and Co take place. This interpretation is used in the work of Bergman et al. [37] -where bcc Fe clusters surrounded by a bcc Co layer are studied by first principles- to account for the enhancement of the spin moment of the Fe atoms and supported by the similarities between bulk bcc Co density of states (DOS) and the Fe local DOS at the surface. Remarkably, the calculated moment for the interface bcc Co spin and orbital moments are 1.80 μ_B and 0.14 μ_B respectively, [37] close to the values obtained in our work. Bear in mind that although Bergman et al. studied Fe clusters in a Co matrix, the interface effect is likely to be the same, irrespective of other mechanisms taking place. Nevertheless, a detailed study of a similar system to the one described in this work is, to the best of our knowledge, lacking in the literature and it is needed to elucidate the precise origin of the high magnetic moments.

Regarding the atomic Co spin and orbital magnetic moments measured by XMCD, 1.97 μ_B and 0.24 μ_B, respectively, are higher than the 1.55 μ_B and 0.153 μ_B measured from bulk hcp Co [38]. Indeed, bulk bcc Co is expected to exhibit a spin magnetic moment 12 % higher than the hcp counterpart due to their different DOS and Fermi level position, which also relates to the stability of their magnetic moment in different non-collinear spin structures [39]. Yet, total energy DFT calculations have shown values of the spin magnetic moment for bulk bcc Co that are

still lower (around 1.75 μ_B) than the value reported here [40,41]. Interestingly, DFT calculations on the surface of a bcc Co (001) thin films by Lee et al. [41] revealed a spin magnetic moment of 2.12 μ_B in the surface of a monolayer, which reduced to the 1.94 μ_B in thicker films and to the bulk value in deeper layers. They ascribed these values to the minority d-electron band splitting at the surface and an increase in the exchange splitting value. The similarity of the spin magnetic moment of the surface layer in bcc Co thin films with the one reported here suggests and supports the previous idea about the crucial role of the Fe-Co interface. Note that the total moment of 2.21 μ_B, which represents a 30 % increase compared to the bulk value, is likely to be an underestimate, as we know there is a small degree of oxidation of the Co nanoparticles.

It is also likely that there is a co-operative effect in the magnetisation as the cobalt content increases, i.e., as the nanoscale Co/Fe interface grows, whereby the enhancement of the Co magnetic moment increases the magnetisation in the Fe that feeds back onto the Co. This is indicated by the magnetometry data in Fig. 6 that shows that at a very low Co content (1.3 at%, sample 2) the magnetic moment per atom is indistinguishable, within the error, from pure Fe, but the magnetisation grows rapidly when the Co concentration increases to 11.4 at%.

We expect that there is still some way to go towards optimising the performance of the material. For example, it would be interesting to study the effect of changing the diameter of the deposited nanoparticles. In addition, it has been shown that having a degree of interfacial mixing at the Fe/Co interface may increase the atomic magnetic moments [36]. Such interdiffusion could be tailored via annealing films similar to those studied here. Moreover, the samples presented here could be made magnetically soft enough for certain applications by exploring different approaches, e.g. by using a suitable underlayer [42], by annealing [43,44] or by introducing trace elements into the films, as is done in bulk FeCo alloys [45], which would all be readily achievable using the vacuum deposition method described here. Finally, it is important to emphasise that the high magnetic performance is due to the nanostructure within a relatively thick film and does not depend on the thickness of the film. Thus, scale up is purely a technological rather than fundamental problem.

5. Conclusion

In this study, Fe-rich FeCo nanostructured thin films have been synthesized by combining gas-phase cluster deposition and atomic vapour deposition. Although this system was already known to the scientific community, we have confirmed both its magnetisation above the bulk FeCo Slater-Pauling curve (up to an 18 % increase with respect to the bulk value) and the reproducibility in both the synthesis method and its magnetic behaviour. By careful and conservative error analysis in both the mass determination and magnetometry evaluation, our study provides improved confidence in the "exceptionally high magnetisation" of the FeCo nanostructured films.

Using different techniques, we were able to show that the nanoparticles maintain their integrity within the film, providing nanostructured interfaces (between Fe and Co) absent of voids or pores. Using XAS and XMCD, we were able to elucidate the magnetism of the Co nanoparticles -showing a bcc structure with the Fe lattice constant- which exhibit an atomic magnetic moment at least 30 % higher than the bulk value. Nanostructured FeCo is therefore a very promising material with respect to future applications. It is hoped that the present study will stimulate further investigation towards the optimisation of its application-relevant magnetic properties.

CRediT authorship contribution statement

Larissa S.I. Veiga: Writing – review & editing, Investigation. **Benito Santos Burgos:** Writing – review & editing. **Hanqing Liu:** Investigation. **Christopher Binns:** Writing – review & editing, Writing – original draft, Validation, Supervision, Project administration, Investigation, Funding acquisition, Formal analysis, Data curation, Conceptualization. **Shengfu Yang:** Writing – review & editing, Investigation, Conceptualization. **Toby Bird:** Writing – review & editing, Investigation. **Andrew Pratt:** Writing – review & editing, Supervision, Resources. **José Ángel De Toro:** Writing – review & editing, Supervision, Funding acquisition. **Sarnjeet S. Dhesi:** Writing – review & editing, Investigation. **Peter Stephen Normile:** Writing – review & editing. **Connor Fields:** Investigation. **David Hesp:** Investigation. **Jack Pearce:** Investigation. **Maha Alotaibi:** Investigation. **Raúl López-Martín:** Writing – review & editing, Writing – original draft, Investigation, Formal analysis, Data curation.

Declaration of Competing Interest

The authors declare that they have no known competing financial interests or personal relationships that could have appeared to influence the work reported in this paper.

Data availability

Data will be made available on request.

Acknowledgements

This work was supported by the Junta de Comunidades de Castilla-La Mancha [SPBLY/21/180501/000226] and Ministerio de Ciencia, Innovación y Universidades [ATHENS: PID2022–142267NB-I00]. R. Lopez-Martin acknowledges his predoctoral research grant co-funded by the European Social Fund [2020-PREDUCLM-16730]. S. Yang acknowledges support from the UK Engineering and Physical Sciences Research Council (EPSRC) [EP/V027255/1] and the Leverhulme Trust [RPG-2020–152]. The authors would like to thank Diamond Light Source for supporting the experiments.

References

[1] P. Weiss, The magnetic properties of the alloys of the ferromagnetic metals: iron-nickel, nickel-cobalt, cobalt-iron, Trans. Faraday Soc. 8 (1912) 149–156, https://doi.org/10.1039/TF9120800149.
[2] R.S. Sundar, S.C. Deevi, Soft magnetic FeCo alloys: alloy development, processing, and properties, Int. Mater. Rev. 50 (2005) 157–192, https://doi.org/10.1179/174328005X14339.
[3] C. Binns, Single Nanoparticle Devices, in: Introd. to Nanosci. Nanotechnol., 2nd ed., Wiley, 2022, pp. 211–218.
[4] H.J. Richter, The transition from longitudinal to perpendicular recording, J. Phys. D. Appl. Phys. 40 (2007) R149, https://doi.org/10.1088/0022-3727/40/9/R01.
[5] K. Vijayakumar, R. Karthikeyan, S. Paramasivam, R. Arumugam, K.N. Srinivas, Switched reluctance motor modeling, design, simulation, and analysis: a comprehensive review, IEEE Trans. Magn. 44 (2008) 4605–4617, https://doi.org/10.1109/TMAG.2008.2003334.
[6] G. Scheunert, O. Heinonen, R. Hardeman, A. Lapicki, M. Gubbins, R.M. Bowman, A review of high magnetic moment thin films for microscale and nanotechnology applications, Appl. Phys. Rev. 3 (2016) 11301, https://doi.org/10.1063/1.4941311.
[7] J.M.D. Coey, Ferromagnetism and Exchange. Magn. Magn. Mater., Cambridge University Press, Cambridge, 2009, pp. 144–152.
[8] A. Díaz-Ortiz, R. Drautz, M. Fähnle, H. Dosch, J.M. Sanchez, Structure and magnetism in bcc-based iron-cobalt alloys, Phys. Rev. B 73 (2006) 224208, https://doi.org/10.1103/PhysRevB.73.224208.
[9] J.M.D. Coey, K. O'Donnell, Qi Qinian, E. Touchais, K.H. Jack, The magnetization of alpha"Fe16N2, J. Phys. Condens. Matter 6 (1994) L23, https://doi.org/10.1088/0953-8984/6/4/001.
[10] Y. Iwasaki, R. Sawada, E. Saitoh, M. Ishida, Machine learning autonomous identification of magnetic alloys beyond the Slater-Pauling limit, Commun. Mater. Y. Iwasaki, R. Sawada, E. Saitoh, M. Ishida, Mach. Learn. Auton. Identif. Magn. Alloy. beyond Slater-Pauling Limit, Commun, Https//Doi.Org/10.1038/S43246-021-00135-0. 2, Mater 2 (2021) 31, https://doi.org/10.1038/s43246-021-00135-0.
[11] C. Binns, K.N. Trohidou, J. Bansmann, S.H. Baker, J.A. Blackman, J.-P. Bucher, D. Kechrakos, A. Kleibert, S. Louch, K.-H. Meiwes-Broer, G.M. Pastor, A. Perez, Y. Xie, The behaviour of nanostructured magnetic materials produced by depositing gas-phase nanoparticles, J. Phys. D. Appl. Phys. 38 (2005) R357, https://doi.org/10.1088/0022-3727/38/22/R01.

[12] C. Binns, P.B. Howes, S.H. Baker, H. Marchetto, A. Potenza, P. Steadman, S. S. Dhesi, M. Roy, M.J. Everard, A. Rushforth, Loss of long-range magnetic order in a nanoparticle assembly due to random anisotropy, J. Phys. Condens. Matter 20 (2008) 55213, https://doi.org/10.1088/0953-8984/20/5/055213.
[13] S. Flohrer, G. Herzer, Random and uniform anisotropy in soft magnetic nanocrystalline alloys (invited), J. Magn. Magn. Mater. 322 (2010) 1511–1514, https://doi.org/10.1016/j.jmmm.2009.07.087.
[14] I.M.L. Billas, A. Châtelain, W.A. de Heer, Magnetism from the atom to the bulk in iron, cobalt, and nickel clusters, 1682 LP – 1684, Science 265 (80) (1994), https://doi.org/10.1126/science.265.5179.1682.
[15] S.E. Apsel, J.W. Emmert, J. Deng, L.A. Bloomfield, Surface-enhanced magnetism in nickel clusters, Phys. Rev. Lett. 76 (1996) 1441–1444, https://doi.org/10.1103/PhysRevLett.76.1441.
[16] M.B. Knickelbein, Adsorbate-induced enhancement of the magnetic moments of iron clusters, Chem. Phys. Lett. 353 (2002) 221–225, https://doi.org/10.1016/S0009-2614(02)00024-6.
[17] F.W. Payne, W. Jiang, J.W. Emmert, J. Deng, L.A. Bloomfield, Magnetic structure of free cobalt clusters studied with Stern-Gerlach deflection experiments, Phys. Rev. B 75 (2007) 94431, https://doi.org/10.1103/PhysRevB.75.094431.
[18] S.H. Baker, C. Binns, K.W. Edmonds, M.J. Maher, S.C. Thornton, S. Louch, S. S. Dhesi, Enhancements in magnetic moments of exposed and Co-coated Fe nanoclusters as a function of cluster size, J. Magn. Magn. Mater. 247 (2002) 19–25, https://doi.org/10.1016/S0304-8853(02)00090-2.
[19] G.N. Iles, S.H. Baker, S.C. Thornton, C. Binns, Enhanced capability in a gas aggregation source for magnetic nanoparticles, J. Appl. Phys. 105 (2009) 24306, https://doi.org/10.1063/1.3067761.
[20] A. Harres, M. Mikhov, V. Skumryev, A.M.H. de Andrade, J.E. Schmidt, J. Geshev, Criteria for saturated magnetization loop, J. Magn. Magn. Mater. 402 (2016) 76–82, https://doi.org/10.1016/j.jmmm.2015.11.046.
[21] J. Stöhr, H. König, Determination of spin- and orbital-moment anisotropies in transition metals by angle-dependent x-ray magnetic circular dichroism, Phys. Rev. Lett. 75 (1995) 3748–3751, https://doi.org/10.1103/PhysRevLett.75.3748.
[22] G. van der Laan, Relation between the angular dependence of magnetic x-ray dichroism and anisotropic ground-state moments, Phys. Rev. B 57 (1998) 5250–5258, https://doi.org/10.1103/PhysRevB.57.5250.
[23] S.H. Baker, M. Roy, S. Louch, C. Binns, Atomic structure in magnetic cluster assembled Fe/Co films as determined from extended absorption fine structure, J. Phys. Condens. Matter 18 (2006) 2385, https://doi.org/10.1088/0953-8984/18/8/004.
[24] L. Cabral, F.H. Aragón, L. Villegas-Lelovsky, M.P. Lima, W.A.A. Macedo, J.L.F. Da Silva, Tuning the magnetic properties of FeCo thin films through the magnetoelastic effect induced by the Au underlayer thickness, ACS Appl. Mater. Interfaces 11 (2019) 1529–1537, https://doi.org/10.1021/acsami.8b14736.
[25] H.S. Jung, W.D. Doyle, J.E. Wittig, J.F. Al-Sharab, J. Bentley, Soft anisotropic high magnetization Cu/FeCo films, Appl. Phys. Lett. 81 (2002) 2415–2417, https://doi.org/10.1063/1.1510163.
[26] G. Herzer, Modern soft magnets: amorphous and nanocrystalline materials, Acta Mater. 61 (2013) 718–734, https://doi.org/10.1016/j.actamat.2012.10.040.
[27] J.M. MacLaren, T.C. Schulthess, W.H. Butler, R. Sutton, M. McHenry, Electronic structure, exchange interactions, and Curie temperature of FeCo, J. Appl. Phys. 85 (1999) 4833–4835, https://doi.org/10.1063/1.370036.
[28] F. Jiménez-Villacorta, C. Prieto, Y. Huttel, N.D. Telling, G. van der Laan, X-ray magnetic circular dichroism study of the blocking process in nanostructured iron-iron oxide core-shell systems, Phys. Rev. B 84 (2011) 172404, https://doi.org/10.1103/PhysRevB.84.172404.
[29] V. Papaefthimiou, T. Dintzer, V. Dupuis, A. Tamion, F. Tournus, A. Hillion, D. Teschner, M. Hävecker, A. Knop-Gericke, R. Schlögl, S. Zafeiratos, Nontrivial redox behavior of nanosized cobalt: new insights from ambient pressure x-ray photoelectron and absorption spectroscopies, ACS Nano 5 (2011) 2182–2190, https://doi.org/10.1021/nn103392x.
[30] J.T. Lau, J. Rittmann, V. Zamudio-Bayer, M. Vogel, K. Hirsch, P. Klar, F. Lofink, T. Möller, B. v. Issendorff, Size dependence of ${L}_{2,3}$ branching ratio and $2p$ core-hole screening in X-Ray absorption of metal clusters, Phys. Rev. Lett. 101 (2008) 153401, https://doi.org/10.1103/PhysRevLett.101.153401.
[31] N.D. Telling, G. van der Laan, S. Ladak, R.J. Hicken, Spin polarization and barrier-oxidation effects at the Co/alumina interface in magnetic tunnel junctions, Appl. Phys. Lett. 85 (2004) 3803–3805, https://doi.org/10.1063/1.1812383.
[32] B.T. Thole, P. Carra, F. Sette, G. van der Laan, X-ray circular dichroism as a probe of orbital magnetization, Phys. Rev. Lett. 68 (1992) 1943–1946, https://doi.org/10.1103/PhysRevLett.68.1943.
[33] P. Carra, B.T. Thole, M. Altarelli, X. Wang, X-ray circular dichroism and local magnetic fields, Phys. Rev. Lett. 70 (1993) 694–697, https://doi.org/10.1103/PhysRevLett.70.694.
[34] A. Langenberg, K. Hirsch, A. Ławicki, V. Zamudio-Bayer, M. Niemeyer, P. Chmiela, B. Langbehn, A. Terasaki, B. v Issendorff, J.T. Lau, Spin and orbital magnetic moments of size-selected iron, cobalt, and nickel clusters, Phys. Rev. B 90 (2014) 184420, https://doi.org/10.1103/PhysRevB.90.184420.
[35] D.C. Douglass, A.J. Cox, J.P. Bucher, L.A. Bloomfield, Magnetic properties of free cobalt and gadolinium clusters, Phys. Rev. B 47 (1993) 12874–12889, https://doi.org/10.1103/PhysRevB.47.12874.
[36] Y. Xie, J.A. Blackman, Magnetism of iron clusters embedded in cobalt, Phys. Rev. B 66 (2002) 85410, https://doi.org/10.1103/PhysRevB.66.085410.
[37] A. Bergman, E. Holmström, A.M.N. Niklasson, L. Nordström, S. Frota-Pessôa, O. Eriksson, Magnetism of Fe clusters embedded in a Co matrix from first-principles theory, Phys. Rev. B 70 (2004) 174446, https://doi.org/10.1103/PhysRevB.70.174446.
[38] C.T. Chen, Y.U. Idzerda, H.-J. Lin, N.V. Smith, G. Meigs, E. Chaban, G.H. Ho, E. Pellegrin, F. Sette, Experimental confirmation of the X-ray magnetic circular dichroism sum rules for iron and cobalt, Phys. Rev. Lett. 75 (1995) 152–155, https://doi.org/10.1103/PhysRevLett.75.152.
[39] L.M. Sandratskii, J. Kübler, Local magnetic moments in bcc Co, Phys. Rev. B 47 (1993) 5854–5860, https://doi.org/10.1103/PhysRevB.47.5854.
[40] D.J. Singh, Magnetism in bcc cobalt, Phys. Rev. B 45 (1992) 2258–2261, https://doi.org/10.1103/PhysRevB.45.2258.
[41] J.I. Lee, C.L. Fu, A.J. Freeman, Electronic structure and magnetism of metastable bcc Co(001), J. Magn. Magn. Mater. 62 (1986) 93–100, https://doi.org/10.1016/0304-8853(86)90739-0.
[42] X. Liu, H. Kanda, A. Morisako, The effect of underlayers on FeCo thin films, J. Phys. Conf. Ser. 266 (2011) 12037, https://doi.org/10.1088/1742-6596/266/1/012037.
[43] D. Hunter, W. Osborn, K. Wang, N. Kazantseva, J. Hattrick-Simpers, R. Suchoski, R. Takahashi, M.L. Young, A. Mehta, L.A. Bendersky, S.E. Lofland, M. Wuttig, I. Takeuchi, Giant magnetostriction in annealed Co1−xFex thin-films, Nat. Commun. 2 (2011) 518, https://doi.org/10.1038/ncomms1529.
[44] T. Sourmail, Evolution of strength and coercivity during annealing of FeCo based alloys, Scr. Mater. 51 (2004) 589–591, https://doi.org/10.1016/j.scriptamat.2004.05.028.
[45] M. Ma, X. Zhao, X. Sun, J. Jiang, W. Shao, L. Zhen, Microstructure evolution and strengthening mechanism of FeCo-1.5V0.5Nb0.4 W soft magnetic alloy rolled strip with high yield strength and low coercivity, Acta Mater. 268 (2024) 119793, https://doi.org/10.1016/j.actamat.2024.119793.